1986

Heat Transfer Effects During Cold Dense Gas Dispersion: Wind-Tunnel Simulation of Cold Gas Spills

R. N. Meroney
Professor.

D. E. Neff
Research Associate.

Fluids Mechanics and Wind Engineering,
Civil Engineering Department,
Colorado State University,
Fort Collins, CO 80523

Wind-tunnel concentration data were obtained for continuous area releases of ambient temperature Freon–air mixtures, cold N_2, cold CO_2, and cold CH_4 clouds. Heat transfer and humidity effects on model concentration distributions were significant for methane plumes when surface Richardson numbers Ri_* were large (i.e., low wind speed and high boiloff rate conditions). At field scales heat transfer and humidity will still play a role in the dispersion of methane spill cases, but plume dilution and liftoff are not expected to be as exaggerated as for the model cases.

1.0 Introduction

Storage and transport of flammable hydrocarbon fuels with subambient boiling points have potential hazards associated with inadvertent release into the atmosphere. Fuels in this category include liquefied natural gas (LNG), ethane, propane, and butane (LPG). At ambient temperature, these liquids boil rapidly and form cold gas clouds that are negatively buoyant often until the cloud dilutes below its lower flammability limit (LFL). Previous analyses of laboratory experiments modeling dense gas plumes have not discussed thermal effects on plume mixing behavior, so new model experiments were performed to study the effect of heat transfer on cold dense cloud dispersion.

Wind-tunnel tests were performed at model scale to determine heat transfer effects on a LNG plume. Since a LNG plume is heavier than air at boiloff conditions, it is expected to disperse as a negatively buoyant cloud. Negatively buoyant plumes were simulated in the wind tunnel by ambient temperature heavy gas or cooled lighter gases, such that the specific gravity of the source gas is equal to that of LNG vapor at boiloff.

The measured concentrations were scaled to account for differences in moles of cold methane gas versus the source moles of alternative model source gas. Heavy gases were introduced into the wind tunnel via a constant-area source mounted flush with the wind-tunnel floor. Mean gas concentrations and mean temperatures were evaluated at various locations both downwind and upwind of the source. Concentration samples were analyzed using a gas chromatograph. Temperatures were evaluated throughout the plume with a thermocouple multiplexer system. Plume structure was determined from the concentration and temperature profiles.

1.1 Dense Gas Kinematics. Continuous source plumes arise in situations such as pipeline ruptures without valve closedown or releases of very large quantities of cryogenic liquid gas onto land or water in the presence of wind. Puttock et al. [10] describe a number of field tests which produced continuous dense gas plumes.

Initially, continuous cold plumes exhibit rapid horizontal spreading caused by the excess hydrostatic head of the cloud. The result is a low wide plume, the effect being more pronounced at low wind speeds. In instances of low and moderate wind speed, the plume will even extend upwind, although the gas will eventually lose its initial upwind momentum and be rolled back over or around the source. A consequence of the velocity reversal of gas upwind from the source is the generation of a horseshoe-shaped vortex, which bounds the laterally parabolic gas cloud.

The initial gravitationally induced collapse of the cloud converts potential energy into kinetic energy, part of which is in turn transmitted to the surrounding ambient fluid, where it is dissipated by turbulence. The energy transfer primarily occurs at the head of the spreading cloud and in its wake. The cloud will reach a point where the gravitational spreading velocity is small compared to the mean ambient wind velocity. Presumably, significant amounts of air will be entrained due to mixing, and the cloud will be advected downwind at ambient air speeds. Hence, the cloud takes on a parabolic shape with plume depth being symmetric about the center line.

Surface heating of the plume and heat from condensation of water vapor entrained with the air reduce the plume's negative buoyancy. The result is a decrease in the instantaneous Richardson number thereby enhancing both dispersion by atmospheric turbulence and the subsequent downwind advection of the plume. As the buoyancy becomes positive and the plume less stably stratified, it may actually lift off the ground surface. For large spills of LNG under moderate wind conditions significant liftoff does not seem to occur before the lower flammability limit is attained.

For small field spills or laboratory-scale spills surface heating effects will be exaggerated. When a large Rayleigh number condition exists (i.e., large temperature differences or large cloud depth) it is hypothesized that surface heat transfer will be proportional to $h_s L^3/U$, where L is the characteristic length scale of the plume, U is the characteristic velocity scale, and h_s is the convection heat transfer coefficient, which is not a strong function of the length scale. The thermal capacity of a gas cloud will vary as $\rho C_p L^3$, where ρ is plume density and C_p is specific heat capacity. The ratio of surface heat transport to thermal capacitance (the Stanton number St) is $h_s/(\rho C_p U)$. Since the wind speed for stratified flows is scaled by the ratio of buoyancy to inertial forces or a Froude number, $U^2/g'L$, and the surface heat transfer is likely to include a free convection component small model-scale plumes will see a temperature increase (or density decrease) which does not scale to the field equivalent. Cold model plumes will entrain air faster and lift off before the comparable field situation [1].

1.2 Simulation of Dense Cloud Motion. The structure of the adiabatic atmospheric boundary layer may be adequately simulated in the laboratory if a minimum Reynolds number, $\mathrm{Re} = u_* z_0/\nu$, exceeds 2.5, where u_* is friction velocity, z_0 is surface roughness, and ν is kinematic viscosity; otherwise the

Contributed by the Heat Transfer Division for publication in the JOURNAL OF HEAT TRANSFER. Manuscript received by the Heat Transfer Division December 7, 1984. Paper No. 84-WA/HT-78.

CEP83-84RNM-DEN-16

boundary layer grows over an unrealistically smooth surface. In addition similarity between approach wind and turbulence profiles is generally necessary. Simulation of heavy cloud motion additionally requires that various plume mass ratios, force ratios, energy ratios, and property ratios be equal for both model and prototype. Neff and Meroney [8] considered various scaling arguments for isothermal dense gas plumes, and they concluded that equivalence of specific gravity ratio, $SG = \rho_0/\rho_a$; flux Froude number, $Fr = U_a^3 L/(g'_0 Q)$; and volume flux ratio, $Q/(U_a L^2)$ are sufficient to assure similarity.

The scaling considerations mentioned above are equally applicable to the scaling of cold heavy clouds. However, in the case of thermal plumes additional considerations must be made to insure that the model plume's specific gravity history is similar to that of its full-scale counterpart. Processes which affect specific gravity history include:

- thermal expansion or contraction of the plume due to differences in the molar specific heat capacity of the plume source gas and air
- release of latent heat during the entrainment of humid air
- heat transfer by conduction, convection, or radiation across plume boundaries

For the case of a thermal plume whose molar specific heat capacity is different from air, such as an LNG vapor plume, the modeling of the density history variation within the plume can only be approximate. For a given molar dilution the specific gravity after adiabatic mixing of the LNG plume will slightly exceed that for isothermal modeling, and the plume cross section will be slightly smaller. The release of latent heat through the entrainment of humid air can also have a very significant effect on the density history of a thermal plume. Latent heat will reduce the plume's negative buoyancy during its initial mixing period, but the plume density may increase later as the moisture re-evaporates, when the plume temperature exceeds the atmospheric dew point.

2.0 Data Acquisition and Analysis

The cold gas experiments were modeled in the Environmental Wind Tunnel (EWT) at Colorado State University. This atmospheric boundary-layer wind tunnel has a test section 3.66 m wide, 2.28 m tall, and 17.0 m long. Vortex generators and a wall trip at the test-section entrance produced a boundary layer about 1 m deep at the experiment location 10.0 m downwind of the entrance.

A constant area source (Fig. 1*a*) was mounted flush with the floor of the EWT. Two heavy isothermal and three cooled gases were released continuously from the source. A heat exchanger (Fig. 1*b*) was used to establish the proper thermal conditions of the source gases. The heat exchanger used nitrogen as the cooling fluid both in gaseous and in liquid form. A pool of liquid nitrogen was maintained around the source gas plenum, so that little if any source gas heating would occur until the gas became exposed to the ambient atmosphere. The source gas was cooled in a gas-to-gas counterflow heat exchanger. Temperatures were regulated by adjusting coolant gas temperatures and flow rate, and release temperatures were set within ±5 K. All source gases contained a known percentage of a hydrocarbon tracer. An oil smoke was used to visually define ambient temperature gas

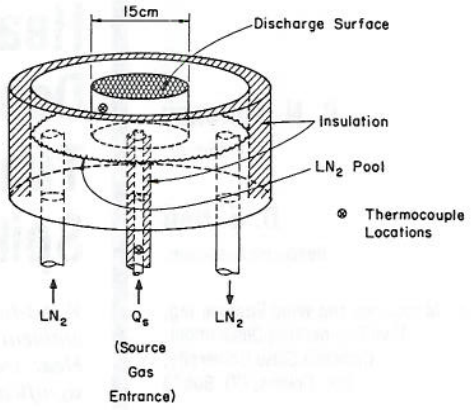

Fig. 1(*a*) Source plenum construction details

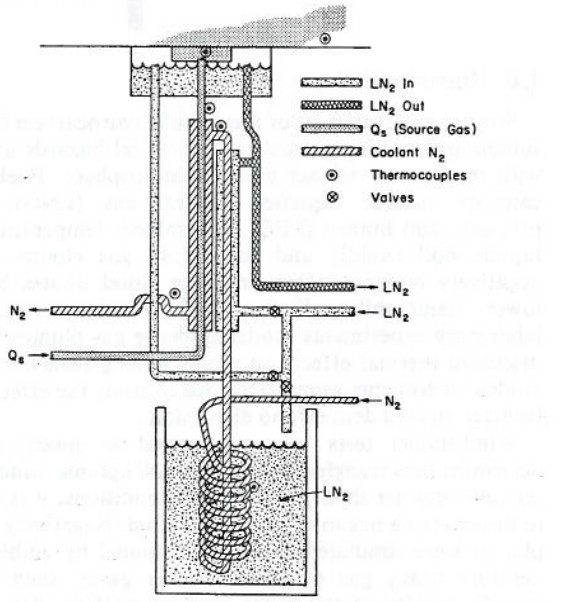

Fig. 1(*b*) Schematic diagram cryogenic heat exchanger to cool source gases and plenum

Nomenclature

C = concentration
C_f = skin friction coefficient
C_p = specific heat capacity (mass)
C_p^* = specific heat capacity (molar)
E = entrainment ratio = w_e/u_*
g' = modified gravitational constant = $g(\Delta\rho/\rho)$
Gr = Grashof number
H = cloud depth
h_s = surface heat transfer coefficient
K = dimensionless concentration coefficient
L = characteristic length scale
l_b = buoyancy length scale = $g'Q/U_R^3$
MW = molecular weight
Nu = Nusselt number
Q = source strength
R = universal gas constant
Re = Reynolds number
Ri_* = Richardson number
SG = specific gravity
St = Stanton number
T = temperature
U = wind speed
u_* = friction velocity
w_e' = entrainment velocity
z_0 = surface roughness length
ρ = density
ν = kinematic viscosity
Δ = temperature difference
ϕ = humidity

Subscripts

0 = source conditions
a = ambient conditions
m = model conditions
p = prototype conditions
R, ref = reference conditions

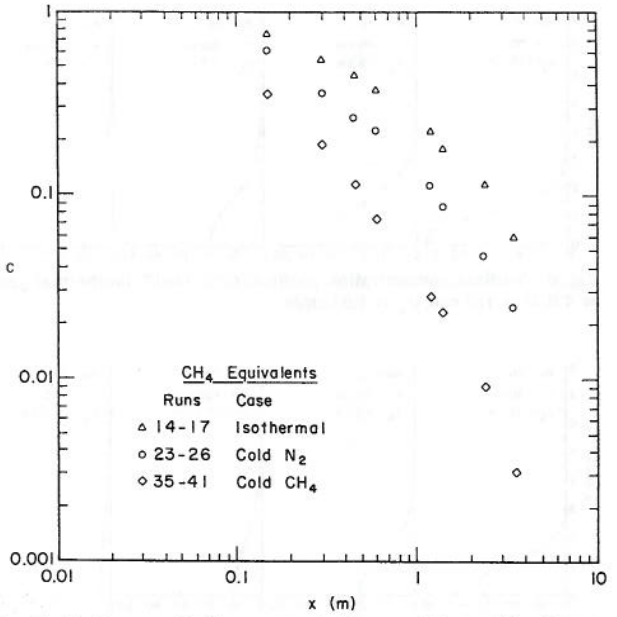

Fig. 2 Surface centerline concentration variation with distance, $l_b \sim 4.0$, $Q = 130$ ccs, $u_* = 1.85$ cm/s

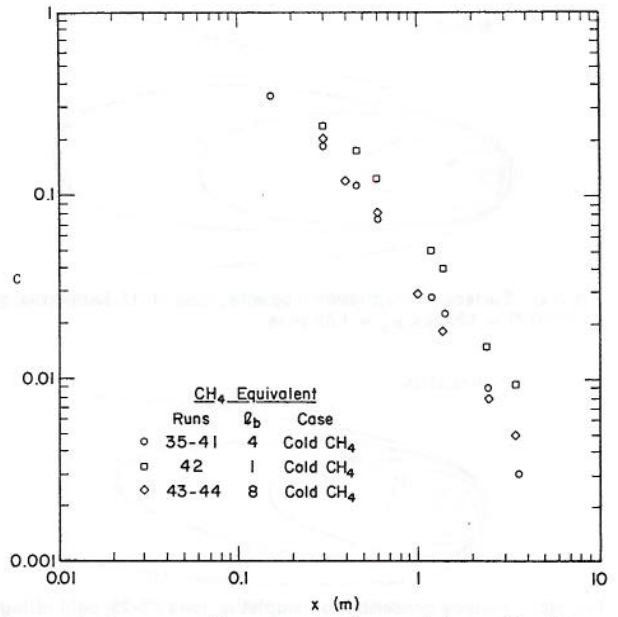

Fig. 4 Surface centerline concentration variation with distance, methane runs, $l_b = 1, 4$, and 8

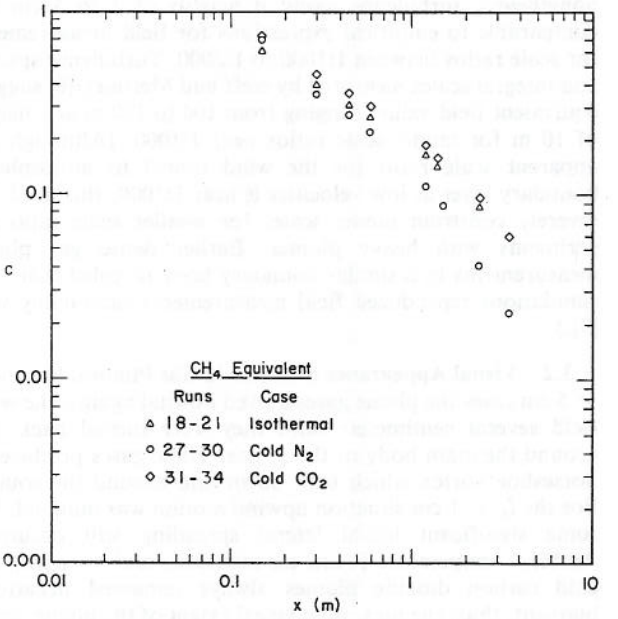

Fig. 3 Surface centerline concentration variation with distance, $l_b \sim 4.0$, $Q = 223$ ccs, $u_* = 3.20$ cm/s

plume behavior, while cold gas plume boundaries could be observed as a result of background humidity condensation within the plume. Correlations of plume outlines with concentration isopleths suggest the smoke edges reflect a concentration near 0.1 percent.

The approach wind velocity profile, reference wind speed conditions, and turbulence were measured with a Thermo-Systems 1050 anemometer and 1210 hot-film probe. Multipoint calibration procedures suggest that velocities were measured within 5–10 percent of their actual values. A thermocouple multiplexer (Model Digitrend 22) monitored up to 45 copper/constantan thermocouples once each minute during each experiment. In addition one fast response (0.025 mm diameter) thermocouple was placed 15 cm downwind of the source and 0.5 cm above the ground and monitored continuously.

Average concentrations were measured at 81 stations for each simulated spill. The floor in the vicinity of the plumes was always flat and smooth with no obstacles to cause wake effects. Runs 1–12 were performed to determine the reaction of plume behavior to a range of initial conditions. Sample tubes for vertical and surface concentrations were arranged above the floor and may have produced wakes which caused additional dilution. In later tests, Runs 13–44, sampling tubes were mounted flush with the surface and connected to the sampler via a hollow chamber beneath the wind-tunnel floor. To obtain a series of vertical profiles, experiments were replicated up to five times, and only data at or upwind of any concentration probe rake should be considered accurate. The replications provided redundant data that defined concentration variability between test runs. Samples were drawn from the tunnel in 50 sample sets over a period of 5 min at a rate of about 6 cc/min. Such sampling times are equivalent to 10–20-min averages at field scales. Individual samples were then evaluated for tracer gas concentration by a flame-ionization detector in a gas chromatograph (Hewlett Packard Model 5710A). The error in measured concentration is imposed by the detector sensitivity, source strength and sampling uncertainties, and the background concentration of tracer within the wind tunnel. Background concentrations were measured and subtracted from all data; hence, final model concentrations are accurate to ±10 percent over most of the detection range.

3.0 Test Program and Data

The cold dense plume measurement program was designed to provide a basis for the analysis of heat transfer effects on plume dispersion, the evaluation of plume scaling laws, and to assist in the development of and verification of numerical models. Source gas mixtures were prepared to provide gases which were all initially heavy; but they were either ambient temperature, cold with molar specific heat capacity ratio $(C_p^*)_0/(C_p^*)_a = 1.0$, or cold with $(C_p^*)_0/(C_p^*)_a > 1.0$. Thus one could evaluate whether dilution and plume dimensions resulted from adiabatic entrainment, heat transfer effects, or unbalanced thermal expansion. Since wind-tunnel velocity and heat-exchanger temperatures sometimes drifted from the ideal set points, the actual conditions examined are noted in Table 1. Detailed data tables are available in the report by Andriev et al. [1].

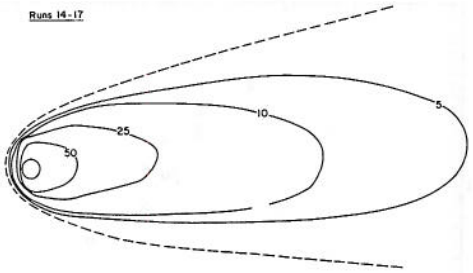

Fig. 5(a) Surface concentration isopleths, runs 14–17, isothermal gas, l_b = 4.0, Q = 130 ccs, u_* = 1.85 cm/s

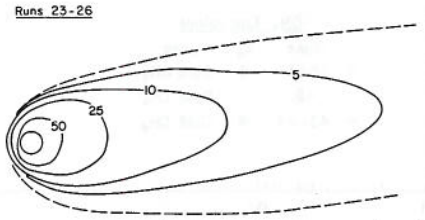

Fig. 5(b) Surface concentration isopleths, runs 23–26, cold nitrogen, l_b = 4.0, Q = 130 ccs, u_* = 1.85 cm/s

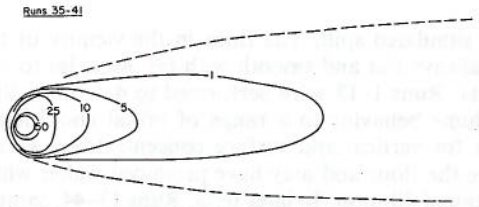

Fig. 5(c) Surface concentration isopleths, runs 35–41, cold methane, l_b = 2.9, Q = 130 ccs, u_* = 1.85 cm/s

Since gravity effects should be a function of buoyancy length scale l_b (or Richardson number), two buoyancy conditions were selected, l_b = 1 cm and l_b = 5 cm, which were expected to produce small and significant buoyancy effects respectively. Under the first condition background turbulence was expected to dominate entrainment very quickly, but under the latter condition gravity spreading and suppression of vertical mixing was expected to persist. Two combinations of initial molecular weight and initial temperatures were arranged for each buoyancy length scale, and wind speeds were selected to produce equal buoyancy length scales (or equal Richardson numbers) under quite different conditions. If equality of Richardson number alone were adequate for proper plume scaling, then in the absence of heat transfer such experiments should produce identical concentration isopleths. If thermal expansion effects are also minimal then the isothermal and cold nitrogen releases could produce coincident concentration isopleths. If heat transfer effects are minimal then the combined cold methane runs could produce coincident dimensionless concentration isopleths K.

3.1 Velocity and Turbulence Environment. Wind tunnel entrance and floor geometries were identical to those examined by Neff and Meroney [8]. Their conclusions concerning the reasonable similarity of the tunnel boundary layer to the atmospheric boundary remain relevant. The mean wind speed profile was found to fit a logarithmic relationship between heights of 1 to 40 cm. Over a wide range of velocities (0.2 to 1.0 m/s) the surface friction coefficient, $C_f/2 = (u_*/U_{ref})^2 = 0.075$, and the surface roughness z_0 was 0.0001 m. Profiles of longitudinal turbulence intensity decay with height from values near 0.25 at the ground. Magnitudes fall off at upper levels faster than equivalent atmospheric profiles;

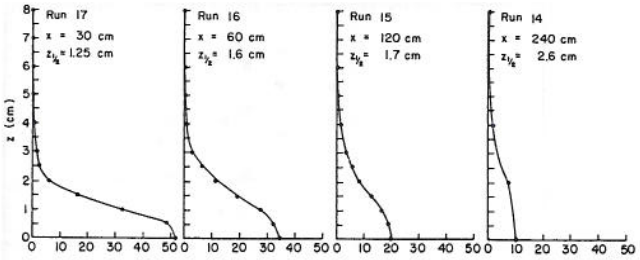

Fig. 6 Vertical concentration profiles, runs 14–17, isothermal gas, l_b = 4.0, Q = 130 ccs, u_* = 1.85 cm/s

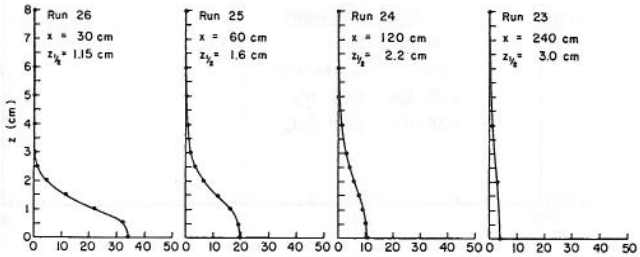

Fig. 7 Vertical concentration profiles, runs 23–26, cold nitrogen, l_b = 4.0, Q = 130 ccs, u_* = 1.85 cm/s

nonetheless, turbulence levels at heights of 1 to 5 cm are comparable to empirical expressions for field measurements for scale ratios between 1:1000 to 1:2000. Turbulence spectra and integral scales measured by Neff and Meroney [8] suggest equivalent field values ranging from 100 to 150 m at a height of 10 m for model scale ratios near 1:1000. (Although the apparent scale ratio for the wind tunnel to atmospheric boundary layer at low velocities is near 1:1000, this need not severely constrain model scales for smaller scale ratio experiments with heavy plumes. Earlier dense gas plume measurements in a similar boundary layer revealed that 1:85 simulations reproduced field measurements reasonably well [7].)

3.2 Visual Appearance of the Cold Gas Plumes. For the l_b = 5 cm cases the plume gases moved upwind against the wind field several centimeters until they were turned back and around the main body of the plume. These gases produced a horseshoe vortex which bent downwind around the source. For the l_b = 1 cm situation upwind motion was minimal, but some significant initial lateral spreading still occurred. Ambient temperature Freon–air mixtures, cold nitrogen, and cold carbon dioxide plumes always remained negatively buoyant; thus, the maximum visual extent of the plume rarely exceeded z = 3 cm at x = 3 m. The stable stratification in the plumes suppressed vertical mixing, so vertical growth followed the character of a Pasquill-Gifford F category plume [9].

The cold methane plumes became positively buoyant after contact with the warm wooden wind-tunnel floor increased plume temperatures. Thus for the l_b = 5 cm cases the plume height grew rapidly within 20 cm of the source. Vertical growth rates appeared to approach Pasquill-Gifford A category rates (unstable atmosphere), and the cloud was 20 cm deep by x = 3 m. In addition the plume lofted above the floor. The vertical rise of the cloud resulted in a narrow ground-level plume width and a very dilute wispy plume. The l_b = 1 cm plume encountered higher wind speeds which suppressed lofting; nonetheless, vertical plume growth exceeded the heavier isothermal and cold nitrogen counterpart plumes.

3.3 Concentration Results. Heat transfer effects may be observed in the relative mixing rates of the various plumes, the resultant variation in centerline concentration with

distance, ground level plume isopleths, and vertical concentration profiles. Concentration data were tabulated in terms of model values, equivalent methane values, and K (dimensionless concentration) values in Appendix D of Andriev et al. [1]. Figures 2–4 show surface centerline methane-equivalent concentrations C versus downwind distance x for selected runs. The isothermal runs 14–17 and 18–21 are essentially coincident; thus, for cases where source vertical momentum is small, buoyancy scale equality is sufficient to assure similarity. Cases where $l_b = 1$ cm also produce similar ambient temperature plume growth.

Cold plumes at $l_b = 1$ or 4 cm do not produce similar behavior. They generally arrange themselves in order of initial temperature, where a lower source temperature subsequently leads to faster dilution rates. An interesting exception is cold carbon dioxide, where the relatively small initial temperature differences from ambient levels and the large specific heat capacity ratio result in centerline concentrations slightly above any isothermal counterpart. The high specific heat capacity of carbon dioxide causes the local specific gravity to remain larger than that of an isothermal counterpart plume of equivalent dilution. This higher density slightly inhibits vertical mixing (see Fig. 3). Methane concentrations displayed in Fig. 4 do not display systematic behavior with buoyancy scale because they involve different source flow conditions. These data will be discussed later in the form of K isopleths.

Typical surface concentration isopleths are plotted in Figs. 5–7 for isothermal, cold nitrogen, and cold methane gases

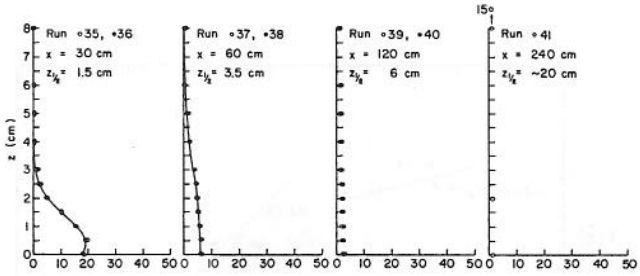

Fig. 8 Vertical concentration profiles, runs 35–41, cold methane, l_b = 2.9, Q = 130 ccs, u_* = 1.85 cm/s

when $l_b = 4$ cm. On each curve the visual extent of the cloud associated with smoke or water droplets is indicated by a dashed line. Visual definition seems to fall off near molar concentrations of one percent. This figure displays upwind plume motion and rapid lateral spreading. The methane plume is comparatively quite narrow, but the concentrations reflect the effects of a buoyant plume rapidly lofting into the air. The plumes continue to grow laterally even after the hydrostatically driven spread velocity $\sqrt{g'H}$ is nearly zero. The growth rate for $x > 2$ m approaches values associated with mixing due to background ambient turbulence.

Vertical concentration profiles were made at $x = 0.3$ to 2.4 m downwind of the source on plume centerline. In no case do we see that the flat, well-mixed regions within the plumes proposed by several authors result from thermal convection. Instead the profiles decay in either a Gaussian or exponential manner. The profiles reported for LNG spills at China Lake showed similar vertical behavior [2].

Cold methane plumes were released under three shear flow conditions (l_b = 1, 4, and 8). Figure 4 displays the dilution of these plumes parallel to wind surface. An alternative data presentation is provided in Fig. 8, where a dimensionless concentration $K = [T_0/T_a]\ [C/(1-C)]\ [U_R L_R^2/Q]$, suggested by Neff and Meroney [8], is plotted versus downwind distance x. This plot automatically normalizes for source variations in volume flow rate or temperature. A band of data associated with isothermal experiments falls above the methane data. Model methane plumes would produce such values if heat transfer effects were absent. The cold methane plumes dilute faster as buoyancy length scale l_b increases. Isothermal data scatter due to sampling tube wake induced turbulence during Runs 1–12. They also vary among Runs 14–17 and 18–21 due to specific gravity effects.

3.4 Temperature Results. During the cold gas runs thermocouples monitored the gas temperatures at selected surface and elevated locations. Temperatures measured are tabulated in Appendix E of Andriev et al. [1]. Local plume temperatures are compared to local concentrations for cold methane plume in Fig. 9. Predicted variations for dry adiabatic and humid adiabatic mixing are noted. These curves are independent of any entrainment model and assume only adiabatic mixing of constant property ideal gases. Predicted

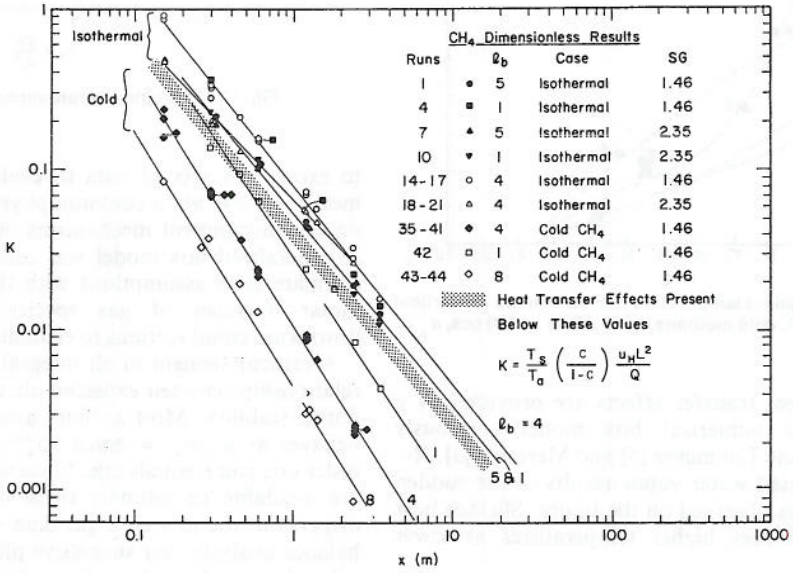

Fig. 9 Dimensionless concentration coefficient variation with distance, isothermal and methane runs; during runs 1–13 the wakes of sampling tube suspended over the cloud artificially reduced plume concentrations

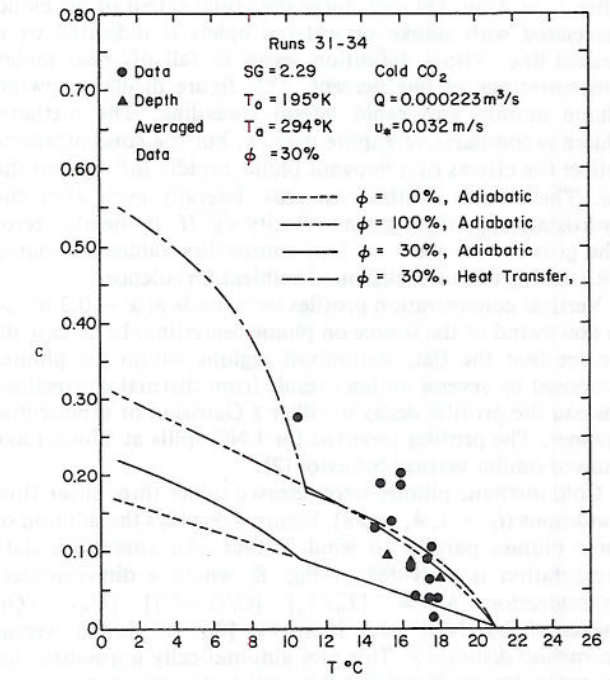

Fig. 10 Concentration against temperature measurements for vertical profile stations, runs 31-34, cold carbon dioxide, l_b = 3.9, Q = 223 ccs, u_* = 3.20 cm/s

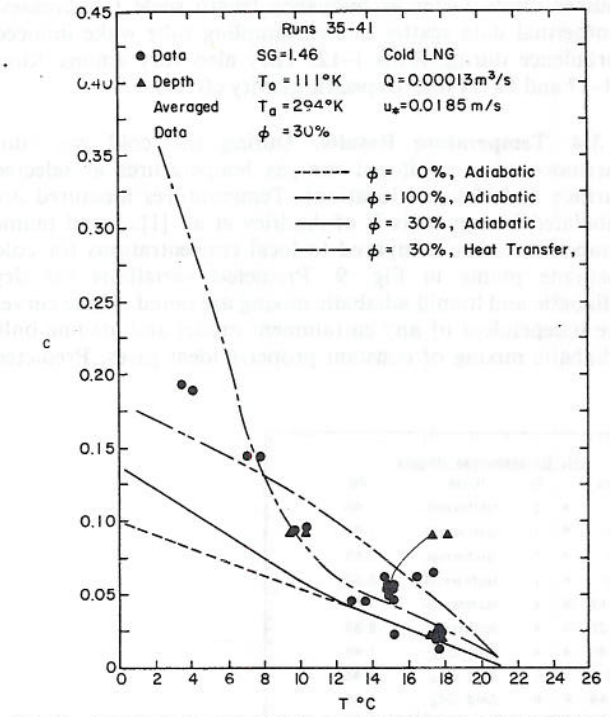

Fig. 11 Concentration against temperature measurements for vertical profile stations, runs 35-41, cold methane, l_b = 2.9, Q = 130 ccs, u_* = 1.85 cm/s

variations including heat transfer effects are provided by a simple depth-averaged numerical box model previously described in Meroney and Lohmeyer [5] and Meroney [3]. Re-evaporation of condensed water vapor results in the sudden change in slope or kinks observed on the figure. Surface heat transfer generally produces higher temperatures at lower dilution levels.

4.0 Discussion of Cold Gas Plume Behavior

The number of analytic and numerical models often seems

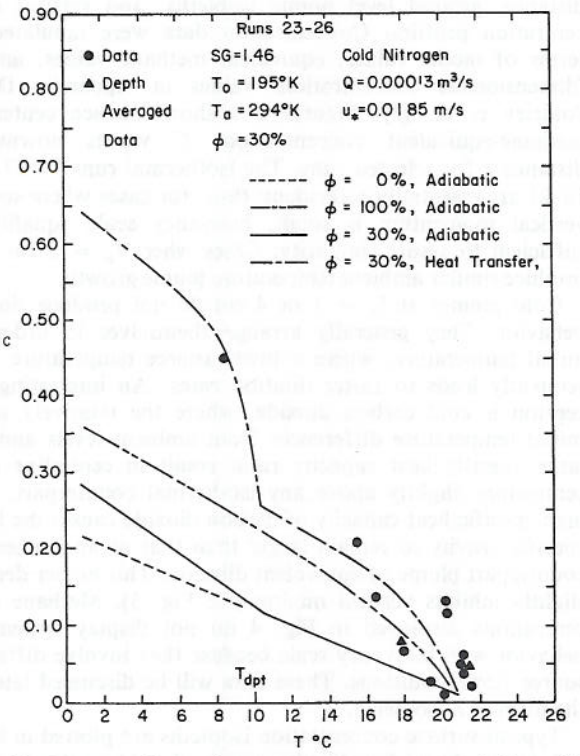

Fig. 12 Concentration against temperature measurements for vertical profile stations, runs 23-26, cold nitrogen, l_b = 4.0, Q = 130 ccs, u_* = 1.85 cm/s

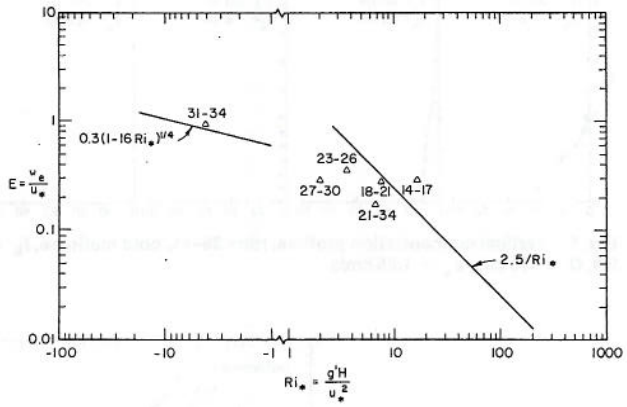

Fig. 13 Entrainment rate versus Richardson number

to exceed the sets of data to evaluate them. Most of these models do contain a common physical foundation, but differ on the entrainment mechanisms or constants recommended. A generalized box model was used by Andriev et al. [1] to compare such assumptions with the experimental data, and molar balances of gas species were performed across downwind cloud sections to estimate entrainment rates.

A critical element in all integral type plume models is the relationship between expected air entrainment rate and local plume stability. Most authors assume that entrainment rate behaves as $w_e/u_* = \text{const}\ \text{Ri}_*^{-n}$, where the constant is of order one and n equals one. Since very few model or field data are available to estimate these coefficients for dense gas dispersion, the new cold gas data were evaluated by a molar balance analysis over successive plume sections. Entrainment velocities calculated from the molar balance are plotted versus measured local Richardson numbers in Fig. 10. The data generally fall close to expected values of const = 2.5 and n = 1; however, due to measurement and evaluation inaccuracies

the scatter is large, and the sections examined did not exhibit the more interesting high Richardson number magnitudes. Picknett [11] and Meroney and Lohmeyer [6] found that dense cloud structure was also influenced by the existence of gravity waves which tend to increase mixing. Perhaps such waves explain the exhibited uncertainties in the measured entrainment rates.

5.0 Conclusions

A large data base detailing heavy gas plume temperatures and concentrations was obtained in an atmospheric boundary layer wind tunnel. Releases included ambient temperature Freon–air mixtures, cold nitrogen, cold carbon dioxide, and cold methane plumes. Heat transfer and humidity effects on model concentration distributions are significant for methane plumes when buoyancy length ratio l_b/L or surface Richardson number Ri_* are large (i.e., low wind speed and high boiloff rate conditions). Ambient temperature mixtures and heavier molecular weight cold simulants always produced higher surface concentrations than the buoyant methane plumes. At field scales heat transfer and humidity are expected to still play a role in the dispersion of methane spill cases, but plume dilution and liftoff will not be as exaggerated as for the model cases.

Cold nitrogen plumes at $l_b = 4$ cm displayed the effects of heat transfer without the complication of specific heat capacity variations between source gas and ambient air. The carbon dioxide plumes, however, required proportionately larger heat transfer to reduce the local buoyancy flux; hence, the cold carbon dioxide plumes resisted mixing even longer than the ambient temperature plume mixtures.

Cold plumes at different buoyancy scales did not display similar patterns of concentration decay. The profiles generally arranged themselves in order of initial temperature, where lower source temperatures resulted in faster dilution rates. (Note exception of carbon dioxide run due to specific heat capacity effects.)

Vertical concentration profiles decay in a Gaussian manner in the vertical for both ambient temperature and cold plumes. The cold plumes mixed vertically more rapidly, since heat transfer destroyed the negative buoyancy and permitted unstable mixing and liftoff.

Acknowledgments

The authors wish to acknowledge support from the Gas Research Institute, Chicago, IL, through Contract No. 5014-352-0203. Mr. George Andriev assisted during measurements and data analysis.

References

1 Andriev, G., Neff, D. E., and Meroney, R. N., "Heat Transfer Effects During Cold Dense Gas Dispersion," Report to Gas Research Institute GRI-83/0082, Chicago, IL, Contract No. 5014-352-0203 to Colorado State University, Fort Collins, CO, 1983.

2 Ermak, D. L., Chan, S. T., Mrogan, D. L., and Morris, L. K., "A Comparison of Dense Gas Dispersion Model Simulations With Burro Series LNG Spill Test Results," *J. Hazardous Materials*, Vol. 6, Nos. 1 & 2, 1982, pp. 129–160.

3 Meroney, R. N., "Transient Characteristics of Dense Gas Dispersion, Part I: A Depth-Averaged Numerical Model," accepted by *J. Hazardous Materials*, 1984.

4 Meroney, R. N., "Transient Characteristics of Dense Gas Dispersion, Part II: Numerical Experiments on Dense Cloud Physics," accepted by *J. Hazardous Materials*, 1984.

5 Meroney, R. N., and Lohmeyer, A., "Prediction of Propane Cloud Dispersion by a Wind-Tunnel-Data Calibrated Box Model," accepted by *J. Hazardous Materials*, 1984.

6 Meroney, R. N., and Lohmeyer, A., "Gravity Spreading and Dispersion of Dense Gas Clouds Released Suddently into a Turbulent Boundary Layer," Report to Gas Research Institute GRI-82/0025, Chicago, IL, Contract No. 5014-352-0203 to Colorado State University, Fort Collins, CO, 1982.

7 Neff, D. E., and Meroney, R. N., "The Behavior of LNG Vapor Clouds: Wind-Tunnel Simulations of 40 m^3 LNG Spill Tests at China Lake Naval Weapons Center, California," Report to Gas Research Institute GRI-80/0094, Chicago, IL, Contract No. 5014-352-0203 to Colorado State University, Fort Collins, CO, 1981.

8 Neff, D. E., and Meroney, R. N., "The Behavior of LNG Vapor Clouds: Wind-Tunnel Tests on the Modeling of Heavy Plume Dispersion," Report to Gas Research Institute GRI-80/0145, Chicago, IL, Contract No. 5014-352-0203 to Colorado State University, Fort Collins, CO, 1982.

9 Pasquill, F., *Atmospheric Diffusion*, Wiley, New York, 1974.

10 Puttock, J. S., Blackmore, D. R., and Colenbrander, G. W., "Field Experiments on Dense Gas Dispersion," *J. Hazardous Materials*, Vol. 6, Nos. 1 & 2, 1982, pp. 13–42.

11 Picknett, R. G., "Field Experiments on the Behavior of Dense Clouds," Report PTN IL 1154/78/1, Chemical Defence Establishment, Porton Down, Wilts., Contract report to the Health & Safety Exec., Sheffield, 1978.

Numerical and Experimental Study of Turbulent Heat Transfer and Fluid Flow in Longitudinal Fin Arrays

D. S. Kadle

E. M. Sparrow
Fellow ASME

Department of Mechanical Engineering,
University of Minnesota,
Minneapolis, MN 55455

Heat transfer from an array of parallel longitudinal fins to a turbulent air stream passing through the interfin spaces has been investigated both analytically/numerically and experimentally. The fins were integrally attached to a heated base plate, while the fin tips were shrouded to avoid leakage. In the analytical/numerical work, a conjugate problem was solved which encompassed turbulent flow and heat transfer in the air stream and heat conduction in the fins and in the base plate. The turbulence model and computational scheme were verified by comparison with experiment. It was found that the local heat transfer coefficients varied along the fins and along the surface of the base plate, with the lowest values in the corners formed by the fin/base plate intersections and the fin/shroud intersections. The numerically determined fin efficiencies did not differ appreciably from those calculated from the conventional pure-conduction fin model. Average Nusselt numbers, evaluated from the experimental data in conjunction with the numerically determined fin efficiencies (for derating the fin surface area), agreed well with those for fully developed heat transfer in a uniformly heated circular tube.

Introduction

Fins are the most commonly used technique for enhancing the rate of heat transfer between a surface and a flowing fluid. In general, fins are treated as a heat conduction problem, while the complex convective heat transfer and fluid mechanic processes in the flow adjacent to the fin and base surfaces have rarely been investigated. The role of convection in fin theory is confined to the introduction of an assumed spatially uniform heat transfer coefficient into the conduction analysis. The assumed uniformity of the heat transfer coefficient is known to be at odds with reality, and the magnitude of the coefficient needed to evaluate the end result of the conduction analysis is often obtained by an educated estimate.

The research described here is a fundamentals-level study of fins which deals both with fin heat conduction and with the turbulent fluid flow and convective heat transfer which occurs in the spaces between the fins. The work includes both experiments and analysis/computation, with the latter encompassing both turbulence modeling and the interactive numerical solution of the fins, the flowing fluid, and the wall to which the fins are attached. Comparisons between the experimental and numerical results are used to establish the validity of the adopted turbulence model and the numerical scheme.

A schematic diagram of the physical situation investigated in both the experimental and the analytical portions of the work is presented in Fig. 1. The figure is a cross-sectional view showing an array of parallel longitudinal fins of rectangular cross section which are integrally attached to a heated wall (hereafter referred to as the base plate). An insulated wall in contact with the fin tips serves to confine the fluid flow to the interfin spaces and, thereby, to create an array of parallel flow passages of rectangular cross section. The experiments were performed for two aspect ratios of the interfin flow passages, namely, $H/W = 3.75$ and 7.5. Air was the heat transfer fluid, and the Reynolds numbers of the airflow ranged from about 5000 to 35,000. In order to facilitate comparisons with the experimental results, the numerical solutions were carried out for the same parametric conditions.

The analytical work was performed for hydrodynamically and thermally developed conditions. The adopted turbulence model took account of the fact that the interfin flow passage was a finite-aspect-ratio rectangular duct rather than a parallel-plate channel, with the resulting velocity distribution being dependent on both cross-sectional coordinates and including corner effects. In the heat transfer portion of the analysis, the energy conservation equations for the fins, the fluid, and the heated base plate were all solved simultaneously. The fundamental nature of this type of analysis eliminates the use of the heat transfer coefficient and thus avoids the aforementioned uncertainties which are related to it. The fin, in common with the fluid and the base plate, was treated on a two-dimensional basis, in contrast to the one-dimensional approach used in the conventional heat conduction analysis of fins.

The results obtained from the combined numerical-experimental study performed here include fin efficiencies, fin temperature distributions, local Nusselt numbers at the surfaces of the fins and the base plate, overall heat transfer rates and Nusselt numbers, and friction factors. The comparisons between the experimental and numerical results will be supplemented by comparisons with literature information for ductflow Nusselt numbers and friction factors.

A survey of the published literature did not reveal any prior work which overlaps with that performed here. In [1], the turbulent flow and heat transfer processes in the fluid passing through an internally finned circular tube were solved numerically, but without simultaneous solution of the fins and the tube wall, which had been assumed to be isothermal. No experimental work was reported in [1]. In [2], a laminar flow analysis, without complementary experiments, was made of a system similar to that of Fig. 1, with the fins being treated by a one-dimensional model.

Contributed by the Heat Transfer Division for publication in the JOURNAL OF HEAT TRANSFER. Manuscript received by the Heat Transfer Division March 13, 1985.